

# 1D thermal modelling of a wheel bearing to investigate energy losses

Márton Kerényi<sup>1\*</sup>, István Goricsán<sup>2</sup>, and Thomas Pitour<sup>3</sup>,

<sup>1</sup> Corresponding author. AUDI HUNGARIA Zrt, Thermo- /Energy Management Development G/GF-1, Audi Hungária út 1., H-9027 Győr, Hungary

<sup>2</sup> AUDI HUNGARIA Zrt, Thermo- /Energy Management Development G/GF-1, Audi Hungária út 1., H-9027 Győr, Hungary

<sup>3</sup> AUDI AG, Energiemanagement I/EG-31, Auto-Union-Straße 1., 85057 Ingolstadt, Germany

**Abstract:** This paper presents the 1D thermal multi-mass simulation of a wheel bearing in order to estimate how the component temperatures affect the energy loss during the Worldwide Harmonized Light Vehicles Test Cycle (WLTC). The simulation model was developed in MATLAB/Simulink on the basis of the conductive and convective heat transfer equations.

The ambient air and bearing components are represented by 7 simplified thermal mass points. The physical quantities necessary to create these points such as area, mass and material of the components were taken from the bearing's 3D computer model. The heat transfer between the individual masses can be determined by setting different values of heat transfer coefficients. In this way it can be observed how much thermal insulation and proper material selection can improve the energy efficiency. The simulation model was created with speed, stability and robustness in mind in order to allow a level of accuracy that meets industrial and scientific expectations.

To validate the model, the simulation results were compared to experimental data. A case study with different heat transfer parameters was concluded to quantify the effect of insulation and so, the energy saving potential.

**Keywords:** 1D simulation, Heat transfer, Insulation, Thermal mass model, Wheel bearing, WLTP driving cycle

## 1 Introduction

During normal operation of a road vehicle, unavoidable resistances are being encountered. These resistant forces, such as the aerodynamic drag, gravitational forces due to road gradient, inertial forces during acceleration and rolling resistance all appear in the form of energy loss as mentioned by [Barrand and Bokar \(2008\)](#); [Zhou et al. \(2022\)](#). The necessity of the reduction of such forces are becoming more significant with the decreasing amount of allowed tank-to-wheel CO<sub>2</sub> emissions and so, fuel consumption imposed by regulations. In the EU, the regulation thresholds are standardised on the basis of driving cycle tests, such as the currently used Worldwide Harmonised Light Vehicles Test Cycle (WLTC) ([Hooftman et al. \(2018\)](#)).

One of the main causes of wasted energy between mechanical parts that are in physical contact with each other and experience relative displacement is friction. Such can be observed inside a wheel bearing assembly. [Khonsari and Booser \(2017\)](#) analysed that the power dissipation in the bearing increases with decreasing component temperature which is primarily influenced by the friction heat and the thermal properties of the materials.

The purpose of this paper is to present a 1D thermal multi-mass simulation that can be used to measure the power dissipation of a wheel bearing during a driving cycle. The parts of the bearing and the relevant nearby components are handled as thermal mass points between which heat transfer connection is built using Fourier's law for conduction and Newton's law of cooling for convection. In the first section, the theoretical considerations behind the model is introduced, then the results of the simulation cycles are compared to the corresponding measurements using statistical metrics as a validation method. In the last section, the different insulation methods are presented and their impact on energy loss due to friction.

## 2 Heat generation inside the bearing

The simulation model is based on a double row deep groove ball bearing. Ball bearings are widely used for places where low energy losses due to friction is prioritised. Still, frictional losses cannot be avoided entirely. During operation, relative motion of the inner and outer rings causes the balls to rotate between them. Without radial load on the bearing, the balls' connection with the rings is at a point or along a line. The work of [Zhaoping and Jianping \(2011\)](#) shows that in the presence of radial load, the contact point transforms into a flatter face as a result of the plastic deformation of the rolling elements caused by stresses according to the Hertzian contact theory. The deformation brings along the increment of the rolling resistance thus more kinetic energy turns into heat. The net effect of friction also appears in the form of a counter torque that opposes the drive torque.

The other source of the frictional torque is viscous friction. As it is pointed out in the work of [Yang and Jeng \(2004\)](#), the friction force between the rotating components and the lubricant oil increases with increasing oil viscosity. However, [Takabi and Khonsari \(2013\)](#) pointed out that oil viscosity decreases as the temperature goes up, proportionally to the speed of the shaft. These relations can be seen in Fig. 1 based on measurement data.

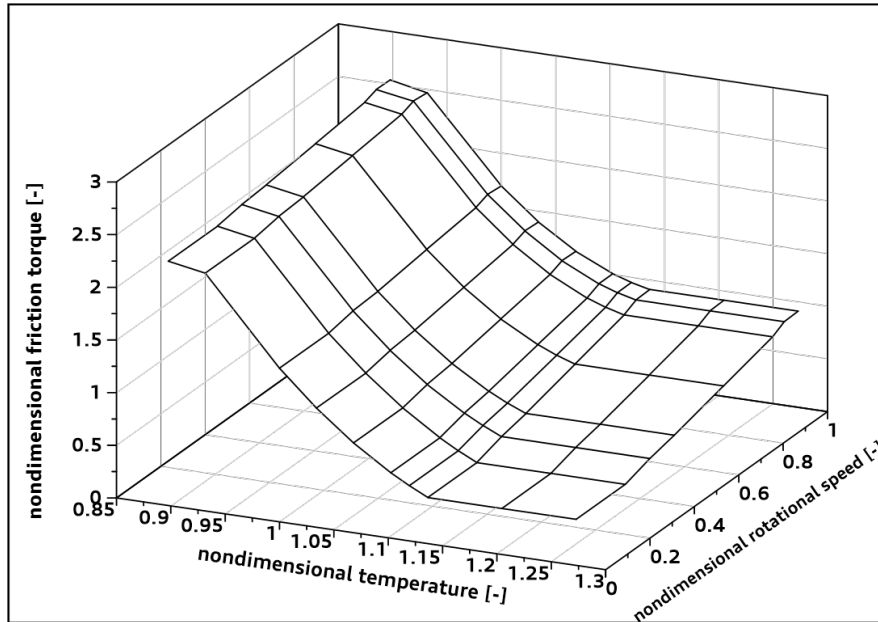


Fig. 1: Experimental relation among the friction torque versus temperature and shaft rotational speed

The exact temperature values in Kelvin have been normalised with a constant temperature also measured in Kelvin. With the friction moment  $M_f$  at different temperature levels and angular velocities ( $\omega$ ), the friction power  $P_f$  can be calculated in kilowatts according to Eq. (1).

$$P_f = M_f \cdot \omega \quad (1)$$

## 2.1 Modeling the heat transfer

The generated heat between the inner and outer rings can dissipate in the form of radiation, conduction and convection (Kovalenko (2021)). By reason of the relative low level of operating temperature, propagation through radiation has not been considered in the paper. The heat is transferred to the neighbouring parts like the wheel hub, inner ring and outer ring based upon the ratio of the surfaces that participate in the heat conduction. Because the outer ring has significantly larger connecting surface to the ambient air compared to the other components, convective heat transfer is only modeled between them. The first stage of the heat transfer process is shown in Fig. 2.

The friction heat between the rings is transferred to the wheel hub and to both rings via conduction. The balls were considered as parts of the outer ring and in the model they form a single part with their masses combined. A similar method is used by Takabi and Khonsari (2013) in their model regarding the mass of the cage and balls. According to our method the cage around the balls was not considered due to the low mass and low heat storage capability. The heat propagation is distributed further in Fig. 3a.

The inner ring is pressed onto the wheel hub and supported by the shoulder of the driven shaft so there are two surfaces and directions where heat can be transferred. The hub is heated directly by the source of the heat and by the inner ring. The brake disc is supported by an annular surface of the hub through which conduction can take place. The hub is fixed on the driven shaft by a spline connection and by an end plate. Both the net surface of the spline teeth and the annular surface of the plate were considered in the calculations. It needs to be mentioned that due to the relative large mass of the brake disc and shaft, their initial temperature is modeled so that they remain constant in time, unaffected by the heat transfer process. The negative feedback contains the amount of heat in kilojoules that the hotter object passes on to the part that it is in connection with. The heat flow at the outer ring is modeled in Fig. 3b.

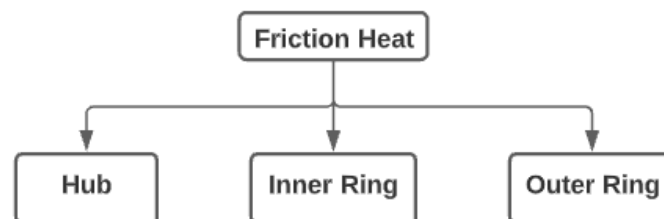


Fig. 2: The distribution of friction heat from the source

The temperature of the outer ring is the reference signal of the model and in this case, the main parameter that indicates the accuracy of the simulation results relative to the measurement data. The outer ring is only getting heat energy from the source and transfers

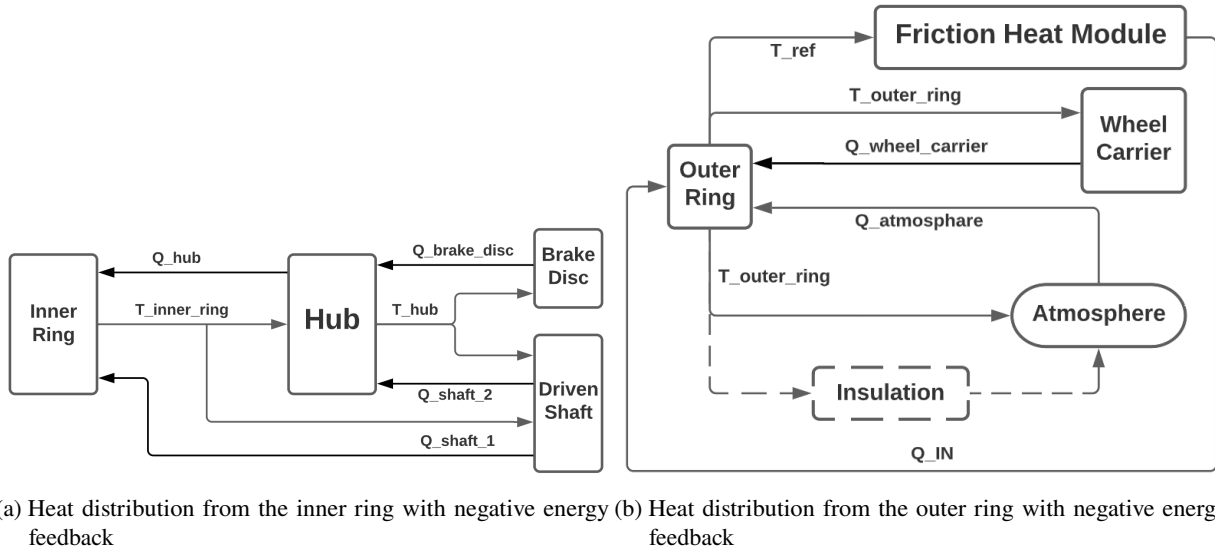


Fig. 3: Heat and energy flow among the bearing components

it directly to the wheel carrier and to the atmosphere through the optional insulation or - if not used - without it. Like in the case of the brake disc and shaft, the temperature of the wheel carrier is also considered time-invariant. The generated amount of friction heat at a given time depends on the temperature of the place where it is being generated. This reference temperature is provided by the signal of the outer ring in a way that it is connected back to the heat generation module at the end of each heat transfer cycle. The basic nature of a 1D simulation model of a physical object with a complex geometry involves necessary usage of methods by whom the model can provide adequately precise results. In order to avoid dealing with complex geometrical shapes, the parts are represented in the model as nodes with thermal connections between them. These nodes contain the value of heat capacity of the particular component with the product of mass ( $m$ ) and specific heat capacity ( $c_p$ ). Additionally, the initial amount of thermal energy ( $Q_0$ ) is known by multiplying the heat capacity with the starting temperature ( $T_0$ ), as shown in Eq. (2) (Flouros (2006)).

$$Q_0 = c_p m T_0 \tag{2}$$

Note that due to the relative small temperature differences the temperature dependence of the specific heat capacity and the heat transfer coefficients have not been taken into account. Heat transfer calculations are solely based on steady-state principles in each simulation cycle.

To guarantee that the accuracy of the heat transfer is not affected by the omission of the geometry, the components are replaced with plain walls with thickness that are calculated from the volume of the part divided by the size of its connecting surface area. The temperature of a component is interpreted to be at the centre of the wall. To model the connection between the nodes, the transition at the contact area was replaced with thermal resistances ( $R_{th}$ ) calculated by the thickness ( $\delta$ ) of the equivalent wall and the thermal conductivity ( $\lambda$ ) of the materials. This way, a similar thermal resistance network can be built just like the one in the work of Mizuta et al. (2003). The calculation of the thermal resistance value of two solid bodies with a shared connecting surface ( $A$ ) is according to Eq. (3).

$$R_{th} = \frac{1}{2A} \left( \frac{\delta_1}{\lambda_1} + \frac{\delta_2}{\lambda_2} \right) \tag{3}$$

The resistances ( $R_{1-8}$ ) at the connecting surfaces are shown in Fig. 4. The abbreviations mean the following:

- $Q_{IN}$ : friction heat generation [ $kJ$ ]
- $T_{\infty}$ : atmosphere temperature [ $K$ ]
- $T_{wc}$ : wheel carrier temperature [ $K$ ]
- $T_{ds}$ : driven shaft temperature [ $K$ ]
- $T_{bd}$ : brake disc temperature [ $K$ ]

The heat flow rate ( $\dot{Q}$ ) between two nodes due to their temperature difference ( $T_1 - T_2$ ) is defined for each time step according to Fourier's law for conduction in Eq. (4) and Newton's law of cooling for convection in Eq. (5).

$$\dot{Q}(t) = \frac{T_1(t) - T_2(t)}{R_{th}} \tag{4}$$

$$\dot{Q}(t) = \alpha A (T_1(t) - T_{\infty}) \tag{5}$$

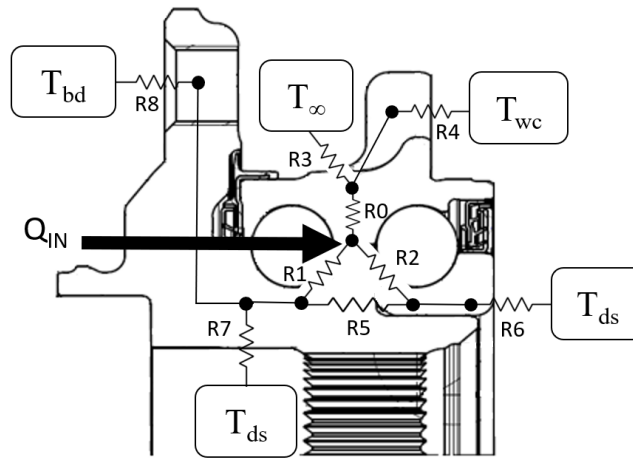


Fig. 4: Schematic network of thermal resistances at the connecting surfaces

Eq. (4) calculates the conductive heat flow rate between two components with the usage of the thermal resistance  $R_{th}$ . In Eq. (5), the convective heat transfer coefficient  $\alpha$  of the fluid can only be defined accurately by experimental measurements since it is not solely determined by the properties of the air but other influencing factors like surface geometry or the nature of the fluid flow. In the heat transfer model, natural convection was modeled, so the  $\alpha$  of the air was set to  $20 \text{ W/m}^2\text{K}$  constant as an estimated value in the case of free convection in gases (Stephan et al. (2010)).

In case of using insulation around the free surface of the outer ring Eq. (6) is used where  $T_1$  is the surface temperature of the ring and  $T_\infty$  is the temperature of the ambient air.

$$\dot{Q}(t) = A \cdot \frac{T_1(t) - T_\infty}{\frac{\delta}{\lambda} + \frac{1}{\alpha}} \tag{6}$$

### 3 Simulation

The goal of the simulation model was to provide a fast, robust and sufficiently accurate method that could be used for estimating the energy losses in the bearing during a driving cycle. The simulation model was built upon data from physical measurements carried out on a test bench. The procedure contained roll-out and constant speed tests during which the speed, braking torque, and the outer ring temperature have been recorded. First, to inspect the convergence of the 1D thermal bearing model, constant speed was given to the heat generation module as input speed for 18 000 seconds. It is displayed in Fig. 5 that the reference temperature settles on a constant value.

One important thing to note is that heat radiation was not considered in the model. The intensive braking sections during a WLTC cycle cause the warming of the brake discs. The net effect of the absorbed heat radiation from the brakes and the dissipated heat on the outer ring’s temperature is balanced out to some extent. Since the approximation of measurement data by the simulation results are within the pre-defined accuracy range, we decided to omit the heat radiation from the model thus avoiding added complexity. The simulation uses a time-discretised solving method, which means that the heat transfer is calculated at each time step during every simulation cycle. This is what gives the transient characteristics of the model results without using transient heat transfer equations.

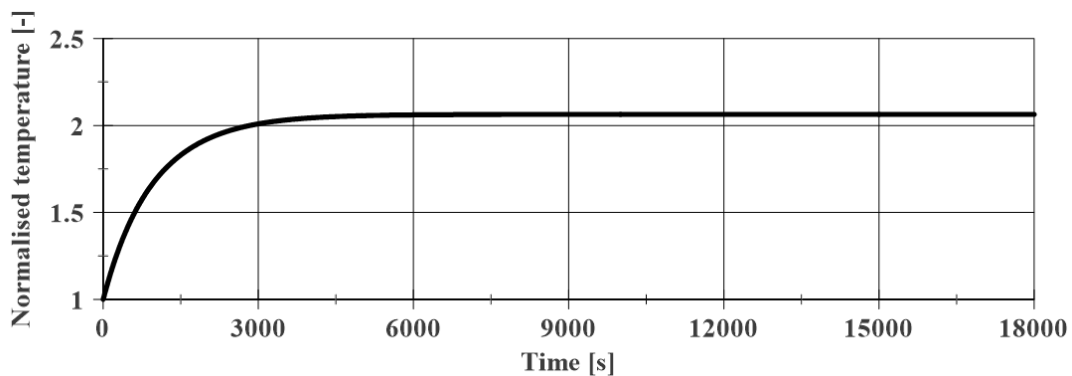


Fig. 5: The outer ring’s temperature transient during an 80 km/h constant speed test

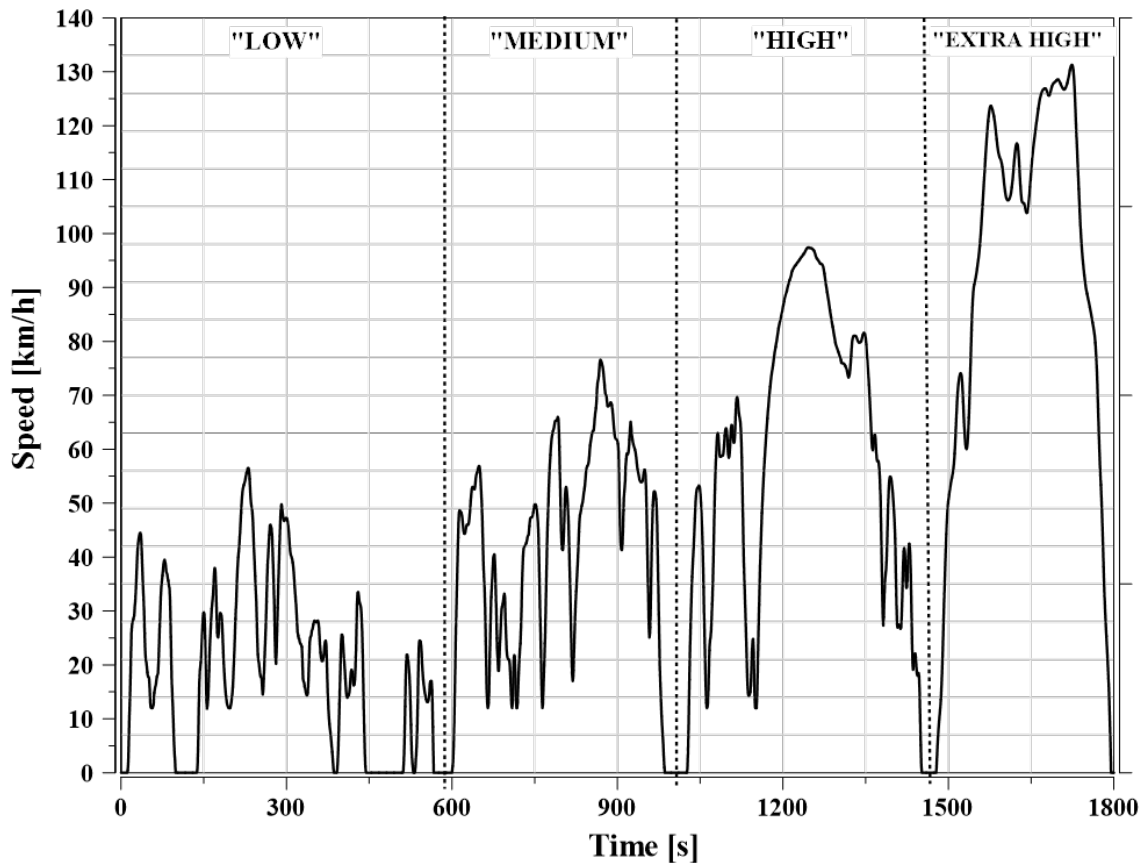


Fig. 6: The vehicle speed curve used during the Class 3b WLTC

### 3.1 Applied test cycle

The frictional energy loss inside the bearing was analysed with the WLTC and its associated Test Procedure (WLTP). The WLTP is an international vehicle legislation and homologation method introduced in 2017 for passenger cars and light trucks (Pavlovic et al. (2016)). The procedure's aim is to provide a more accurate representation of the real world driving emission and fuel consumption values than its predecessor and to make it possible to compare these values internationally. The simulations and measurements in this study use the WLTC cycle for Class 3b vehicles shown in Fig. 6.

The 1800s long cycle contains four sequential ranges in ascending order by the maximum value of the speed in the particular range. The first "Low" region is meant to simulate the real world urban driving scenario while the "Medium", "High" and "Extra High" sections are respectively for the suburban, main road and highway driving scenarios as mentioned in the study of Tutuianu et al. (2015). The test is carried out in laboratory conditions on a chassis dynamometer in standardised 23°C and 14°C ambient temperatures to ensure the procedure's repeatability. This paper also includes the impact of a cold ambient temperature WLTC at -7°C. During each simulation the sampling rate was set to 10Hz.

### 3.2 Applied validation metrics

The accuracy of the simulation model is evaluated by comparing its results to the measurement data. For that, standardised validation metrics were used which provide quantitative characteristics in addition to the qualitative assessment of the curves. The metrics use the set of prediction points ( $P_i$ ) of the simulation result and the set of measured observation points ( $O_i$ ) to define a single value based on which the accuracy can be classified. Both the modeled  $P_i$  and observed  $O_i$  data sets are normalised.

Many recommendations can be found in the studies of Hanna et al. (1993); Hanna (1989) regarding the usage of statistical evaluation metrics for measuring the performance of models. A brief description of the six metrics applied in this paper is introduced in the following.

#### 3.2.1 Hit rate (HR)

The calculation of the Hit rate ( $q$ ) happens according to Eqs. (7) to (8) where the  $n$  number of  $P_i$  and  $O_i$  data point pairs are assessed whether their relative uncertainty ( $D$ ) and the absolute uncertainty ( $W$ ) falls into a user-defined range (Schatzmann et al. (2010)). On its own, a single  $q$  number does not provide information about the under- and over prediction of the simulated points. That is why other metrics are necessary.

$$q = \frac{1}{n} \sum_{i=1}^n N_i \quad (7)$$

$$N_i = \begin{cases} 1 & : \left| \frac{P_i - O_i}{O_i} \right| \leq D \text{ or } |P_i - O_i| \leq W \\ 0 & : \text{else} \end{cases} \quad (8)$$

Assuming an ideal model means  $q = 1$ .

### 3.2.2 Factor of $n$ observations (FACn)

When it comes to measure the effect of infrequent high and low  $O_i$  and  $P_i$  points, the fraction of predictions within a chosen  $n$  number as factor of observations is the most robust measure. It counts those cases when the quotient of the  $P_i$  and  $O_i$  point pairs are within a band given by a lower and upper limit that are calculated with  $n$ . Cases when one or both of  $O_i$  and  $P_i$  are outside of the  $W$  are resulting 0 value according to Eq. (9). The calculation of the final value of  $FACn$  is identical to  $q$  in Eq. (7).

$$N_i = \begin{cases} 1 & : \frac{1}{n} \leq \frac{P_i}{O_i} \leq n \text{ and } (O_i, P_i) \leq W \\ 0 & : \text{else} \end{cases} \quad (9)$$

An ideal model would result into  $FACn = 1$  (Schatzmann et al. (2010)).

### 3.2.3 Fractional bias (FB)

With this linear measure over and under predictions can occur due to the fact that it is based on the mean bias. To solve that, false negative ( $FB_{FN}$ ) and false positive ( $FB_{FP}$ ) values are used to calculate the final value of  $FB$  according to Eq. (10). The  $FB$  indicates only systematic errors.

$$FB = \frac{\sum_i (O_i - P_i)}{0.5 \sum_i (O_i + P_i)} = FB_{FN} - FB_{FP} \quad (10)$$

In case of a perfect model  $FB = 0$  (Schatzmann et al. (2010)).

### 3.2.4 Normalised mean square error (NMSE)

Unlike the  $FB$ , the  $NMSE$  metric is useful to indicate unsystematic errors. The common drawback of the two is the strong influence by the infrequent peaks of data set points. In Eq. (11), the symbols with overline indicate the average over all points in the given data set.

$$NMSE = \overline{(O_i - P_i)^2} / \overline{O_i P_i} \quad (11)$$

A perfect model would have  $NMSE = 0$  (Schatzmann et al. (2010)).

### 3.2.5 Geometric variance (VG) and mean bias (MG)

Similarly to the previously mentioned  $FB$  the  $MG$  also measures mean bias and can be used for indicating systematic errors only. The difference is that the  $MG$  is using logarithmic scale as shown in Eq. (12). As Chang and Hanna (2004) have mentioned, the logarithmic scale used at both metrics helps to provide a more accurate measure when extreme high and low values occur in the data set. Like the  $FB$ ,  $MG$  can also be expressed as an under prediction ( $MG > 1$ ) and an over prediction ( $MG < 1$ ) according to another study by Hanna and Chang (2001).

$$MG = \exp(\overline{\ln(O_i/P_i)}) \quad (12)$$

Just like the  $NMSE$ , the  $VG$  also can be used for both systematic and random errors according to Eq. (13).

$$VG = \exp(\overline{(\ln(O_i/P_i))^2}) \quad (13)$$

For data values of  $O_i$  and  $P_i$  that are zero the absolute deviation  $W$  as lower limit should be used. Both  $MG = 1$  and  $VG = 1$  are obtained if the model is perfect (Schatzmann et al. (2010)).



## 4 Comparison with the measurements

The prediction of the following parameters have been in focus during the simulations:

- Free surface temperature of the outer ring
- Friction power loss as heat

The temperature curves were normalised by the initial temperature of the simulation in Kelvin. The friction power values were normalised by the friction power of a reference bearing in kW. The duration of the simulation is 1800s according to the WLTP with a sampling interval of a constant 0.1s time step. To evaluate the model results relative to the observations, reference signals had to be created. The observation data contains a measurement series of five bearings, each tested two times. As for the temperature parameter, one reference signal was built by calculating the mean of all the ten temperature measurement data series ('*Temperature\_mean\_All*'). The average temperature curve of the two test curves of the bearing measurement that best fitted the model result formed the second reference curve ('*Temperature\_mean\_BestFit*') for the comparison. Note, that at the start of the simulation the bearing component temperatures are set to the same value as the initial temperature following a preconditioning period. The curves are shown in Fig. 7a.

In Fig. 7b. the *HR* is presented between the simulated temperature and the two reference signals. The error boundary is defined by the absolute error  $W = 0.006$  and the relative error  $D = 0.01$ . The acceptance criteria of the matching is set to  $q \geq 0.66$ . It can be stated based on Fig. 7b that all the points of the best fitting measurement are within the borders and it is almost the same with the mean data of all measurements. Table 1 contains the values of the metrics used in the validation.

It can be summarised that just like *HR*, all the other metrics are close to - or the same as - the ideal value, which means that the simulation approximates the observation quite well. The linearity of the model was checked with  $FB \leq 0.15$  condition. For the under and over prediction analysis  $0.9 \leq MG \leq 1.1$  was set for the geometric mean and also 10% deviation was allowed in the case of the geometric variance:  $VG \leq 1.1$ . It can be seen that in the case of  $MG \leq 1$  there is a slight over prediction. The band of the *FACn* is defined with the factor  $n = 1.3$ . The *NMSE* metric is upper-limited by 0.2 ( $NMSE \leq 0.2$ ).

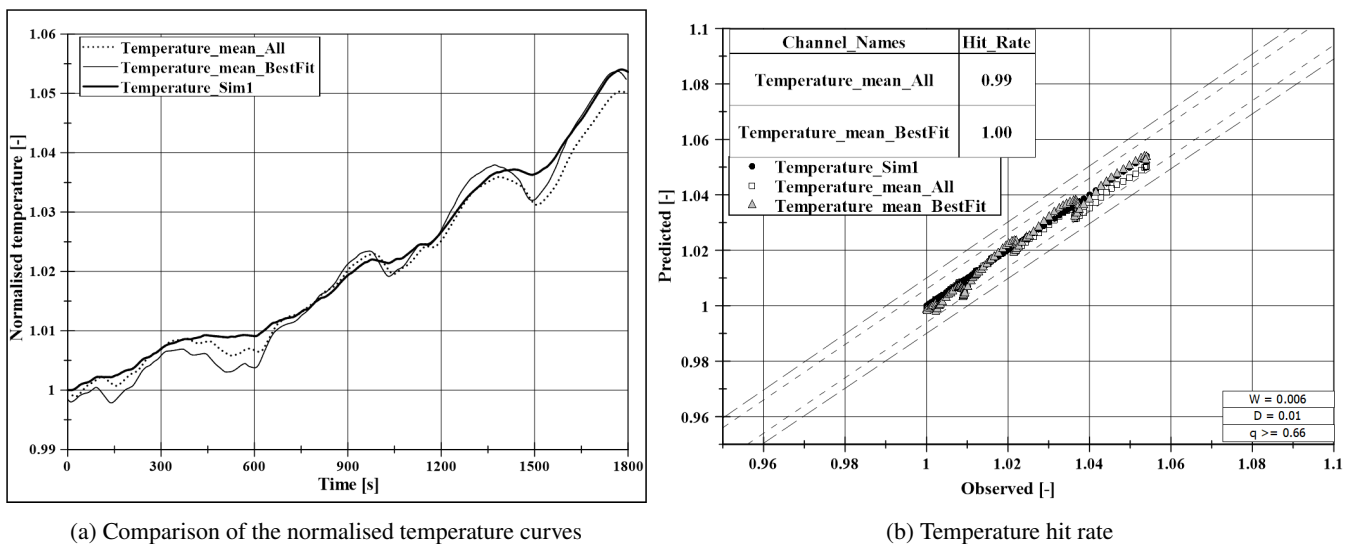


Fig. 7: The three compared temperature curves (a) and their hit rate (b)

Tab. 1: Temperature metrics values

Validation metrics (ideal value)	Condition of acceptance	Temperature mean All	Temperature mean BestFit
HR (1)	$q \geq 0.66$	0.99	1.00
FB (0)	$FB \leq 0.15$	0.0014	0.0161
NMSE (0)	$NMSE \leq 0.2$	0.0005	0.0006
FACn (1)	$0.769 \leq FAC(1.3) \leq 1.3$	0.99	1.00
MG (1)	$0.9 \leq MG \leq 1.1$	0.99	0.98
VG (1)	$VG \leq 1.1$	1.00	1.00

In Fig. 8a. the normalised curves are shown. The path of the friction power curve is following the WLTC's vehicle speed profile. In the analysis of the friction power simulation result, the reference curves shown in Fig. 8b were produced just like the ones in the case of the temperature. In this case, the simulation is somewhat less accurate than it was for the temperature because the friction torque and the speed have uncertainties on their own during the measurement and simulation processes. If the defined boundaries would be less than the uncertainty between the two data sets, the metric would not serve its purpose, so the range limits were set wider for the *HR* by setting  $W = 0.1$  and  $D = 0.25$ . The acceptability condition however remained the same at  $q \geq 0.66$ . According to the results in Table 2 only 66% of the '*mean\_All*' predictions have met the conditions and 71% of the points in the

'mean\_BestFit'. The boundaries of *MG*, *VG* and *FB* were unchanged while the upper limit of *NMSE* and *FACn* was modified to 0.25 and 1.5 respectively. A similar method is used in the evaluation process like the one Goricsán et al. (2011) used in their examination.

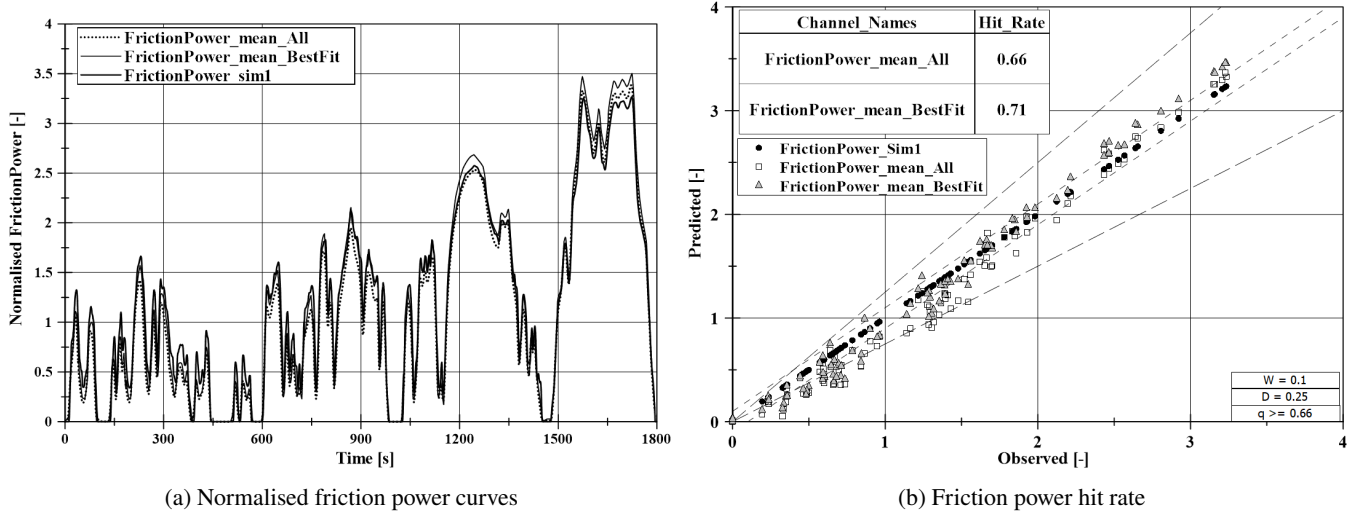


Fig. 8: The three compared friction power curves (a) and their hit rate (b)

Tab. 2: Friction power metrics values

Validation metrics (ideal value)	Condition of acceptance	Friction power mean All	Friction power mean BestFit
HR (1)	$q \geq 0.66$	0.66	0.71
FB (0)	$FB \leq 0.15$	0.1131	0.0988
NMSE (0)	$NMSE \leq 0.25$	0.0214	0.0139
FACn (1)	$0.66 \leq FAC(1.5) \leq 1.5$	0.79	0.84
MG (1)	$0.9 \leq MG \leq 1.1$	0.86	0.93
VG (1)	$VG \leq 1.1$	1.19	1.16

## 5 Effect of insulation

As it was mentioned in Section 2.1. the outer ring transfers heat to the wheel carrier and to the surrounding stationary air. On the other end of the assembly, the brake disc receives heat from the wheel hub. The main purpose of the simulation model was to analyse how and to what extent can the generated friction heat be utilised to decrease the rolling resistance of the bearing. As it was discussed in Section 2, the more heat is kept inside the bearing the more frictional losses decrease. Of course the amount of closed-in heat is upper limited by the material properties and the resulting shorter maintenance intervals. The use of an additional insulating layer on the outer surface of a part decreases the heat transfer capability. In the model this effect was interpreted in the reduction of the heat transfer coefficient of air. In addition to the 23°C WLTC, the simulation was also run with -7°C starting temperature to see how the colder environment affects the bearing's heat balance. Four different cases of insulation were considered in the tests that are listed here and displayed numerically in Table 3.

- partial insulation towards the wheel carrier
- partial insulation towards the brake disc (effects are not discussed in this paper separately)
- partial insulation towards the air
- partial insulation towards all three at the same time

Tab. 3: Heat transfer coefficients for different cases of insulation

Sim. Nr.	$\lambda$ - wheel carrier [W/mK]	$\lambda$ - brake disc [W/mK]	$\alpha$ - air [W/m <sup>2</sup> K]
Sim 1	170	57	20
Sim 2	50	57	20
Sim 3	0.05	57	20
Sim 4	170	57	10
Sim 5	170	57	5
Sim 6	0.05	0.05	5



In the first scenario (*Sim 1*), there is no insulation on any of the components. In the case of *Sim 2* and *Sim 3* the heat transfer towards the wheel carrier is reduced with insulation in two steps. First, from  $170 \text{ W/m}^2\text{K}$  to 50 then to 0.05. Simulations 4 and 5 are the cases when the outer ring's free surface is isolated from the surrounding air represented by halving the value of  $\alpha$  while the other parameters are changed back to their initial values. In the last scenario (*Sim 6*) the insulation is considered to affect the heat flow from the outer ring to the wheel carrier and to the air while on the other side the heat transfer from the hub to the brake disc was also decreased at the same time. The outer ring's surface temperature for each of the six insulation scenarios is displayed in Fig. 9. It can be observed that the curves belonging to *Sim 2-3-4-5* are between the two extreme insulation cases when there was no insulation used (*Sim 1*) and when heat flow was blocked the most (*Sim 6*). Discussion of the separate effect of isolating the hub-brake disc connection is not part of this paper. As it is shown in Fig. 9, the temperature of the outer ring is higher when more friction heat is retained by using insulation (*Sim 6*). As more heat is retained inside the system, the friction and thus the friction power is decreased. The generated friction heat energy is calculated by integrating the friction power over time. The effect of the insulation method on the friction heat generation compared to *Sim 1* is contained in Table 4. According to the results, around 7% less friction heat was generated in the cold test when the most insulation was used. In the European region, the WLTP is also carried out at  $14^\circ\text{C}$  ambient temperature. This is because the time it takes for the engine to warm up is longer in colder ambient temperatures, so the consumed fuel and the  $\text{CO}_2$  emission increases. As it was mentioned earlier, the colder environment also effects the energy losses of the wheel bearing. Therefore, the model was used to investigate the heat generation inside the bearing with  $14^\circ\text{C}$  boundary condition as well. To see the tendencies and correlation, the tests were carried out at every 3 degrees between  $23^\circ\text{C}$  and  $-7^\circ\text{C}$ . Fig 10 displays the outer ring temperature at the end of each simulation. Based on the results it can be clearly seen that the colder initial temperatures increase the final temperature of the outer ring due to larger inner friction. In *Sim 6* the the heat energy is retained with insulation towards the brake disc, wheel carrier and air. In case of a WLTC  $14^\circ\text{C}$ , the generated friction heat was reduced by around 5.6% compared to the case with the same initial temperature but without any insulation.

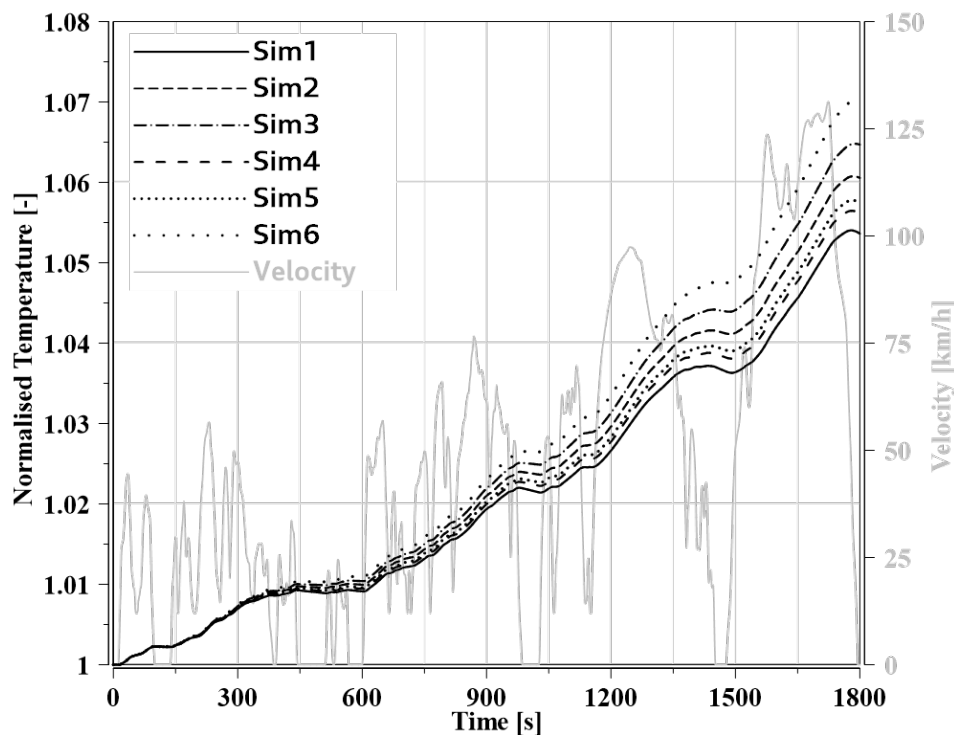


Fig. 9: Normalised surface temperatures of the outer ring with different kinds of insulation

Tab. 4: Change in friction heat generation with insulation compared to *Sim 1*.

Sim. Nr.	WLTC $23^\circ\text{C}$	WLTC $-7^\circ\text{C}$
Sim 2	-2.13 %	-3.08 %
Sim 3	-3.30 %	-4.79 %
Sim 4	-0.79 %	-1.15 %
Sim 5	-1.21 %	-1.75 %
Sim 6	-4.87 %	-7.08 %

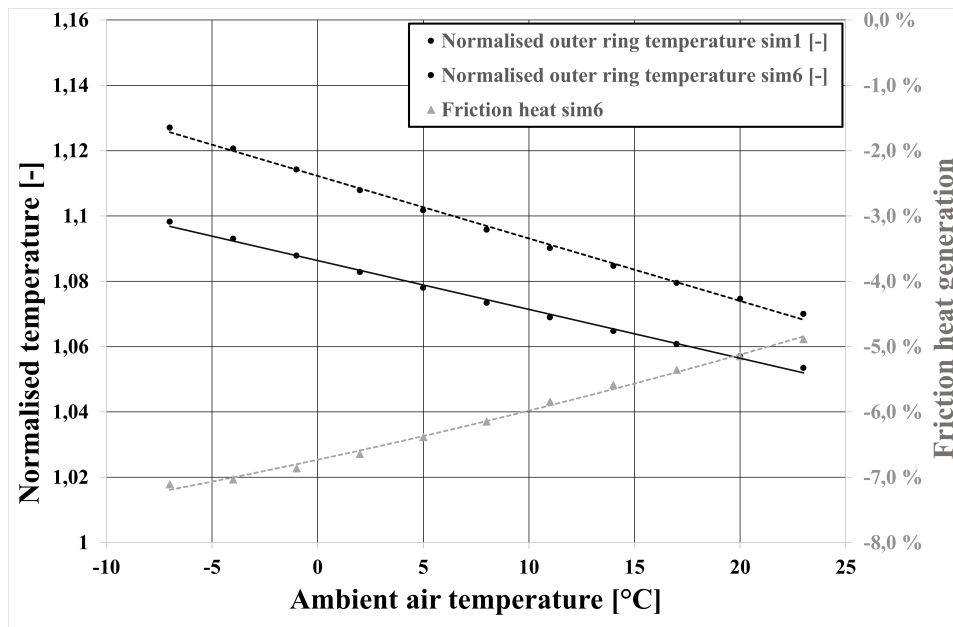


Fig. 10: The effect of decreasing starting temperature on the outer ring's temperature and the heat generation

## 6 Summary

The aim of the paper was to create a 1D TMM model of a wheel bearing assembly that can be used for estimating the energy losses during a WLTC driving cycle. The 1D model contains the bearing components as thermal mass points and the thermal relations between them are governed by the well-known heat transfer equations.

The simulation results were directly compared to measurement data for validation purposes. The most important parameters were the temperature of the outer ring and the frictional energy losses. The paper is focused on the statistical evaluation of the model performance regarding its prediction capability and precision. After that, the effect of different insulation methods were analyzed regarding frictional heat generation. For that, the WLTC driving cycle was used with different ambient temperatures ranging from 23°C to -7°C in steps of 3°C.

The results showed that by applying insulation, a significant proportion of otherwise wasted friction heat energy could be utilised to decrease the frictional resistance of the bearing. Based on the accuracy of the simulation data, the bearing model can be an integral subunit of larger vehicle drivetrain models in the future.

## References

- J. Barrand and J. Bokar. Reducing tire rolling resistance to save fuel and lower emissions. *SAE International Journal of Passenger Cars-Mechanical Systems*, 1(2008-01-0154):9–17, 2008.
- J. C. Chang and S. R. Hanna. Air quality model performance evaluation. *Meteorology and Atmospheric Physics*, 87(1):167–196, 2004.
- M. Flouros. Correlations for heat generation and outer ring temperature of high speed and highly loaded ball bearings in an aero-engine. *Aerospace Science and Technology*, 10(7):611–617, 2006.
- I. Goricsán, M. Balczó, M. Balogh, K. Czáder, A. Rákai, and Cs. Tonkó. Simulation of flow in an idealised city using various cfd codes. *International journal of Environment and Pollution*, 44(1-4):359–367, 2011.
- S. R. Hanna. Confidence limits for air quality model evaluations, as estimated by bootstrap and jackknife resampling methods. *Atmospheric Environment (1967)*, 23(6):1385–1398, 1989.
- S. R. Hanna and J. C. Chang. Use of the kit fox field data to analyze dense gas dispersion modeling issues. *Atmospheric Environment*, 35(13):2231–2242, 2001.
- S. R. Hanna, J. C. Chang, and D. G. Strimaitis. Hazardous gas model evaluation with field observations. *Atmospheric Environment. Part A. General Topics*, 27(15):2265–2285, 1993.
- N. Hooftman, M. Messagie, J. V. Mierlo, and T. Coosemans. A review of the european passenger car regulations—real driving emissions vs local air quality. *Renewable and Sustainable Energy Reviews*, 86:1–21, 2018.
- M. M. Khonsari and E. R. Booser. *Applied tribology: bearing design and lubrication*. John Wiley & Sons, 2017.
- P. Kovalenko. *Heat Transfer on Wheel-Brake System at Critical Thermal Conditions*. PhD thesis, Georgia Institute of Technology, 2021.
- K. Mizuta, T. Inoue, Y. Takahashi, S. Huang, K. Ueda, and H. Omokawa. Heat transfer characteristics between inner and outer rings of an angular ball bearing. *Heat Transfer—Asian Research: Co-sponsored by the Society of Chemical Engineers of Japan and the Heat Transfer Division of ASME*, 32(1):42–57, 2003.

- J. Pavlovic, A. Marotta, and B. Ciuffo. Co2 emissions and energy demands of vehicles tested under the nedc and the new wltc type approval test procedures. *Applied Energy*, 177:661–670, 2016.
- M. Schatzmann, H. Olesen, and J. Franke. Model evaluation case studies: approach and results. *COST 732 report*, 2010.
- P. Stephan, S. Kabelac, M. Kind, M. Holger, D. Mewes, and S. Karlheinz. B1 fundamentals of heat transfer. *VDI Heat Atlas*, pages 15–30, 2010.
- J. Takabi and M.M. Khonsari. Experimental testing and thermal analysis of ball bearings. *Tribology international*, 60:93–103, 2013.
- M. Tutuianu, P. Bonnel, B. Ciuffo, T. Haniu, N. Ichikawa, A. Marotta, J. Pavlovic, and H. Steven. Development of the world-wide harmonized light duty test cycle (wltdc) and a possible pathway for its introduction in the european legislation. *Transportation research part D: transport and environment*, 40:61–75, 2015.
- Y. K. Yang and M. C. Jeng. Analysis of viscosity interaction and heat transfer on the dual conical-cylindrical bearing©. *Tribology transactions*, 47(1):77–85, 2004.
- T. Zhaoping and S. Jianping. The contact analysis for deep groove ball bearing based on ansys. *Procedia Engineering*, 23:423–428, 2011.
- B. Zhou, L. He, S. Zhang, R. Wang, L. Zhang, M. Li, Y. Liu, S. Zhang, Y. Wu, and J. Hao. Variability of fuel consumption and co2 emissions of a gasoline passenger car under multiple in-laboratory and on-road testing conditions. *Journal of Environmental Sciences*, 2022.